ISSN 1674-1056
http://cpb.iphy.ac.cn
http://iopscience.iop.org/cpb
中国物理 B
Chinese Physics
中国物理 Chinese Physics B

PEALD-deposited crystalline GaN films on Si (100) substrates with sharp interfaces

San-Jie Liu(刘三姐), Ying-Feng He(何荧峰), Hui-Yun Wei(卫会云), Peng Qiu(仇鹏), Yi-Meng Song(宋祎萌), Yun-Lai An(安运来), Abdul Rehman(阿布度-拉赫曼), Ming-Zeng Peng(彭铭曾), Xin-He Zheng(郑新和)

Citation: Chin. Phys. B . 2019, 28(2): 026801. **doi:** 10.1088/1674-1056/28/2/026801
Journal homepage: http://cpb.iphy.ac.cn; http://iopscience.iop.org/cpb

What follows is a list of articles you may be interested in

A review for compact model of graphene field-effect transistors

Nianduan Lu(卢年端), Lingfei Wang(汪令飞), Ling Li(李泠), Ming Liu(刘明)
Chin. Phys. B . 2017, 26(3): 036804. **doi:** 10.1088/1674-1056/26/3/036804

Growth condition optimization and mobility enhancement through inserting AlAs monolayer in the InP-based $In_xGa_{1-x}As/In_{0.52}Al_{0.48}As$ HEMT structures

Shu-Xing Zhou(周书星), Ming Qi(齐鸣), Li-Kun Ai(艾立鹍), An-Huai Xu(徐安怀)
Chin. Phys. B . 2016, 25(9): 096801. **doi:** 10.1088/1674-1056/25/9/096801

Effects of grinding-induced grain boundary and interfaces on electrical transportation and structure phase transition in ZnSe under high pressure

Jie Yang(杨洁), Pei Wang(汪沛), Guo-Zhao Zhang(张国召), Xiao-Xue Zhou(周晓雪), Jing Li(李静), Cai-Long Liu(刘才龙)
Chin. Phys. B . 2016, 25(6): 066802. **doi:** 10.1088/1674-1056/25/6/066802

Growth condition optimization and mobility enhancement throughprolonging the GaN nuclei coalescence process of AlGaN/AlN/GaN structure

He Xiao-Guang, Zhao De-Gang, Jiang De-Sheng, Zhu Jian-Jun, Chen Ping, Liu Zong-Shun, Le Ling-Cong, Yang Jing, Li Xiao-Jing, Zhang Shu-Ming, Yang Hui
Chin. Phys. B . 2015, 24(9): 096802. **doi:** 10.1088/1674-1056/24/9/096802

Direct growth of graphene on gallium nitride by using chemical vapor deposition without extra catalyst

Zhao Yun, Wang Gang, Yang Huai-Chao, An Tie-Lei, Chen Min-Jiang, Yu Fang, Tao Li, Yang Jian-Kun, Wei Tong-Bo, Duan Rui-Fei, Sun Lian-Feng
Chin. Phys. B . 2014, 23(9): 096802. **doi:** 10.1088/1674-1056/23/9/096802

PEALD-deposited crystalline GaN films on Si (100) substrates with sharp interfaces*

San-Jie Liu(刘三姐), Ying-Feng He(何荧峰), Hui-Yun Wei(卫会云), Peng Qiu(仇鹏), Yi-Meng Song(宋祎萌), Yun-Lai An(安运来), Abdul Rehman(阿布度-拉赫曼), Ming-Zeng Peng(彭铭曾)†, and Xin-He Zheng(郑新和)‡

School of Mathematics and Physics, Beijing Key Laboratory for Magneto-Photoelectrical Composite and Interface Science, University of Science and Technology Beijing (USTB), Beijing 100083, *China*

(Received 3 November 2017; revised manuscript received 29 November 2018; published online 10 January 2019)

Polycrystalline gallium nitride (GaN) thin films were deposited on Si (100) substrates via plasma-enhanced atomic layer deposition (PEALD) under optimal deposition parameters. In this work, we focus on the research of the GaN/Si (100) interfacial properties. The x-ray reflectivity measurements show the clearly-resolved fringes for all the as-grown GaN films, which reveals a perfectly smooth interface between the GaN film and Si (100), and this feature of sharp interface is further confirmed by high resolution transmission electron microscopy (HRTEM). However, an amorphous interfacial layer ($\sim$ 2 nm) can be observed from the HRTEM images, and is determined to be mixture of Ga_xO_y and GaN by x-ray photoelectron spectroscopy. To investigate the effect of this interlayer on the GaN growth, an AlN buffer layer was employed for GaN deposition. No interlayer is observed between GaN and AlN, and GaN shows better crystallization and lower oxygen impurity during the initial growth stage than the GaN with an interlayer.

Keywords: gallium nitride, PEALD, sharp interface, x-ray reflectivity, high resolution transmission electron microscopy

PACS: 68.35.bg, 68.37.Og, 68.55.Nq **DOI:** 10.1088/1674-1056/28/2/026801

1. Introduction

GaN is an intriguing semiconductor with a direct band gap of 3.4 eV, which makes it useful for various applications, such as ultraviolet (UV) photodetectors,[1] high electron-mobility transistors (HEMTs),[2] light emitting diodes (LEDs),[3,4] and power switching applications.[5] Meanwhile, owing to the high electron velocities, significant thermal stability and radiation resistance, GaN is an attractive candidate for short wavelength optoelectronics and high-power and high frequency electronics.[6,7] Conventional methods for the growth of GaN layers are metalorganic chemical vapor deposition (MOCVD)[8,9] and molecular beam epitaxy (MBE).[10] Both methods necessitate high deposition temperatures, which is neither compatible with the existing complementary metal–oxide–semiconductor (CMOS) technology nor suitable for temperature-sensitive device layers and flexible polymers substrates. In comparison, atomic layer deposition (ALD) is an alternative approach for low-temperature growth of GaN, in which films are prepared using layer-by-layer and self-limiting growth.[11–15] Plasma-enhanced ALD (PEALD) is a modified form of ALD in which energetic radicals assist in accelerating the self-limiting ALD reactants, offering additional merits over ALD such as reduced deposition temperatures and improved material properties.

In recent years, significant efforts have been focused on the growth of GaN using ALD. Biyikli's group has made notable contributions on the low-temperature ALD growth of GaN films with improved electrical properties and crystalline quality.[16–22] The first metal–semiconductor–metal (MSM) ultraviolet photodetectors based on ALD-grown GaN has been demonstrated.[16] Motamedi *et al.* have discussed the influence of the substrate temperature on the properties of GaN thin films grown by ALD[23] and demonstrated a possible route for deposition of single crystal GaN on sapphire.[24] Although Ozgit *et al.*[17] have fabricated polycrystalline GaN films on Si (100), the growth of epitaxial GaN films via ALD on silicon (Si) substrates has not been reported. Since Si is the preferred substrate due to its large diameters at low cost and compatibility with the existing microelectronic technique, the growth of GaN on Si has become a very active field of research. Meanwhile, Si (100) is still the standard substrate for mainstream silicon technology.[25] Therefore, the development of high-quality GaN on Si (100) is necessary for integration with GaN-based devices. However, ALD growth of high-quality GaN on Si (100) is challenging due to the different crystallographic surface symmetries. As the interface between GaN and Si (100) largely determine the quality of the GaN layer, research

*Project supported by the Fundamental Research Funds for the Central Universities (Grant Nos. FRF-BR-16-018A, FRF-TP-17-022A1, and FRF-TP-17-069A1), the National Natural Science Foundation of China (Grant Nos. 61274134 and 51402064), USTB Start-up Program (Grant No. 06105033), China Postdoctoral Science Foundation (Grant No. 2018M631333), Beijing Natural Science Foundation (Grant Nos. 2184112 and 4173077), Beijing Innovation and Research Base Fund (Grant No. Z161100005016095), and the Youth Innovation Promotion Association of Chinese Academy of Sciences (Grant No. 2015387).

†Corresponding author. E-mail: mzpeng@ustb.edu.cn

‡Corresponding author. E-mail: xinhezheng@ustb.edu.cn

© 2019 Chinese Physical Society and IOP Publishing Ltd

on the ALD-grown GaN/Si (100) interface is very meaningful for improving the quality of GaN films on Si (100). However, the study of the interfacial properties between the ALD-grown GaN film and Si (100) substrate is still lacking as far as we know.

In this work, we have studied the structure and chemical states of the GaN/Si (100) interface grown by PEALD. Polycrystalline GaN with wurtzite structure was obtained based on the optimal process parameters. The GaN/Si (100) interface is rather sharp according to the XRR and HRTEM results. HRTEM images also reveal the presence of an amorphous interfacial layer composed of Ga_xO_y and GaN. Upon this amorphous interlayer, an amorphous GaN layer forms, in which oxygen impurity concentration decreases from $\sim 34\%$ to $\sim 11\%$ with the film growth. In comparison, GaN deposited on a PEALD-grown AlN buffer layer shows sharp interface with no interlayer. And GaN shows better crystallinity and lower oxygen impurity during the initial growth stage than the GaN with an interlayer. Moreover, the crystallinity and surface morphology of GaN deposited on Si (100) at different temperatures are characterized.

2. Experimental

GaN thin films were deposited on Si (100) substrates by using Angstrom-dep III PEALD from Thin Film Technologies Ltd. of USA. Triethylgallium (TEG) and $Ar/N_2/H_2$ gas mixture were used as the source of gallium and nitrogen, respectively. Prior to deposition, the substrates were dipped into dilute HF for 2 min and dried with N_2, then processed by sequential ultrasonic agitation in acetone, methanol, and DI-water. Solvent cleaned substrates were then dried with N_2 and loaded immediately onto the reactor chuck in the PEALD system. The process base pressure was adjusted to ~ 0.15 Torr ($1\ \text{Torr} = 1.33322 \times 10^2$ Pa). Once reaching the system base pressure, the substrate chuck was heated resistively to the growth temperature. Twenty minutes at least was needed for temperature to reach a balance. After that, the substrate surfaces were treated with high purity (HP) $Ar/N_2/H_2$ (1:3:6) plasma in an effort to form NH groups, followed by purging the chamber with HP Ar. Subsequently, HP triethylgallium (TEG) was introduced separately for GaN growth. Unreacted TEG and by-products were removed by purging the chamber with HP Ar. Thus, each cycle of GaN growth consists of $Ar/N_2/H_2$ plasma/Ar purge/TEG/Ar purge. Table 1 summarizes the deposition conditions of the GaN films grown by PEALD. As a comparison, an AlN buffer layer was employed. AlN was deposited via PEALD at 275 °C for 50 cycles on *ex situ* cleaned Si (100) and followed by GaN grown at 350 °C. The process parameters of AlN growth was reported in our previous work.[26]

Table 1. Deposition conditions of the GaN films by PEALD.

Precursor 1	TEG (99.999%)
Precursor 2	$Ar/N_2/H_2$ (99.999%)
Carrier gas	Ar (99.999%)
Gas line temperature	60 °C
Flow rate of carrier gas (UHP Ar)	5 sccm
Flow rate of N-precursor	5 sccm
RF power	60 w
RF plasma frequency	13.56 MHz

After deposition, the thickness, density, roughness of GaN films were characterized by x-ray reflectivity (XRR, Smartlab). XRR data of the films were fitted using a 3-layer model ($GaN/Ga_xO_yN_z/Si$). The crystallinity and surface morphology of GaN were analyzed via grazing incidence x-ray diffraction (GIXRD, Smartlab) and Atomic force microscopy (AFM, VEECO D3100). GIXRD measurements were carried out with acceleration voltage of 40 kV and current of 30 mA, and the grazing angle was fixed at 0.5°. Transmission electron microscopy (TEM, JEM-220FS) and x-ray photoelectron spectroscopy (XPS, ESCALAB 250xi) were utilized to investigate the microstructure and chemistry features of the GaN/Si (100) interface.

3. Results and discussion

The GaN deposition conditions are firstly optimized to facilitate the latter interfacial analysis. Deposition rate (growth per cycle, GPC) as a function of temperature is shown in Fig. 1(a). It is seen that GPC decreases as temperature increases from 150 °C to 185 °C, which is due to the condensation of TEG. For temperatures in the range of 200 °C–250 °C, GPC decreases slightly with increasing temperature. A N_2/H_2 plasma saturation curve with constant GPC of ~ 0.97 Å/cycle was obtained at 200 °C (not shown here), which indicates that the growth of GaN at this temperature is self-limiting. A constant GPC of ~ 0.75 Å/cycle obtained within the temperature range of 250 °C–350 °C reveals the self-limiting reaction at these temperatures. When the deposition temperature exceeds 350 °C, GPC increases with elevated temperatures owing to the decomposition of TEG, in which the CVD type of deposition takes place.[15] Hence, the temperature window for this case is determined to be 200 °C–350 °C. The variation of GPC varies with temperature in the ALD window can be explained by the effect of temperature on the number and type of reactive sites present on the surface, since the number of reactive sites decreases with increasing process temperature.[12]

Figure 1(b) shows the GPC as a function of triethylgallium dose and N_2/H_2 plasma, at a deposition temperature of 350 °C. For the triethylgallium saturation curve, the N_2/H_2 plasma is fixed at 30 s. The GPC increases with triethylgallium dose, and then remains constant at ~ 1 Å/cycle when the TEG pulse time is longer than 0.7 s. For the N_2/H_2 plasma

saturation curve [Fig. 1(c)], the triethylgallium dose is fixed at 0.7 s, and the GPC also saturates with the N_2/H_2 plasma above 30 s. The results suggest that the GaN thin films are grown in a self-limiting manner at 350 °C. The effect of purge time on GPC at 350 °C is given in Fig. 1(d). The GPC decreases from 1.0 Å/cycle to 0.9 Å/cycle as the purge time increases from 15 s to 25 s, and then remains constant at this value for longer purge times. Therefore, the optimal deposition parameters in our experiments are: 0.7-s triethylgallium, 30-s N_2/H_2 plasma, and 25-s purge time.

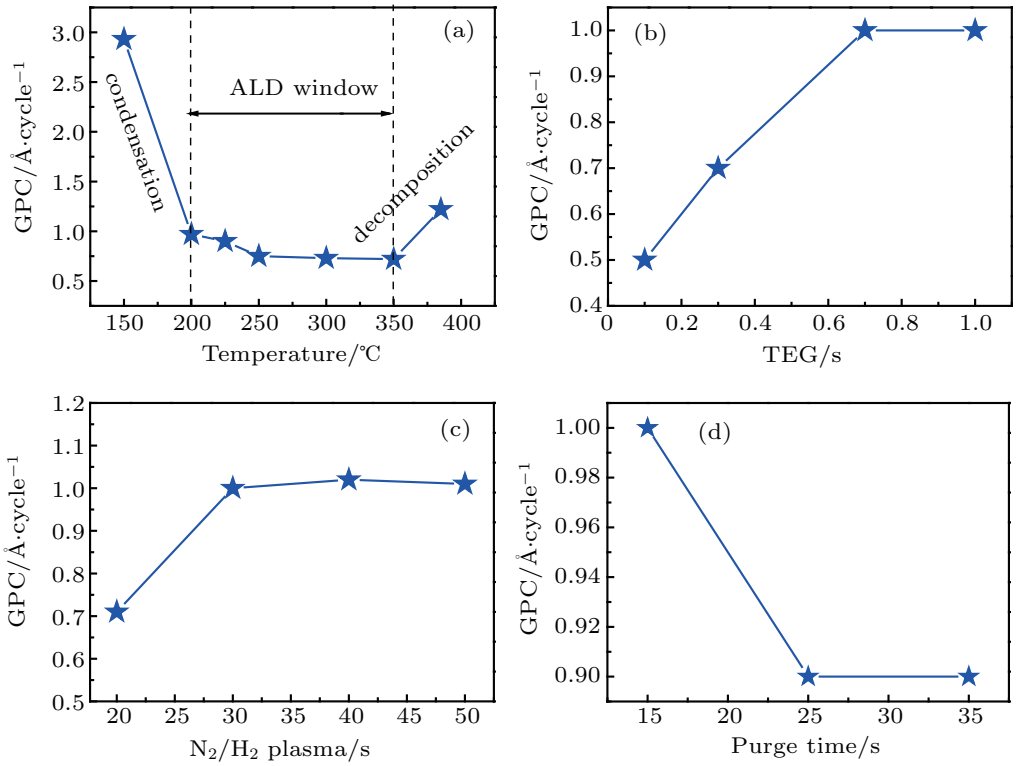


Fig. 1. (a) Deposition rates of GaN thin films at different temperatures. (b) TEG, and (c) N_2/H_2 plasma saturation curves at 350 °C. (d) Deposition rate as a function of purge time.

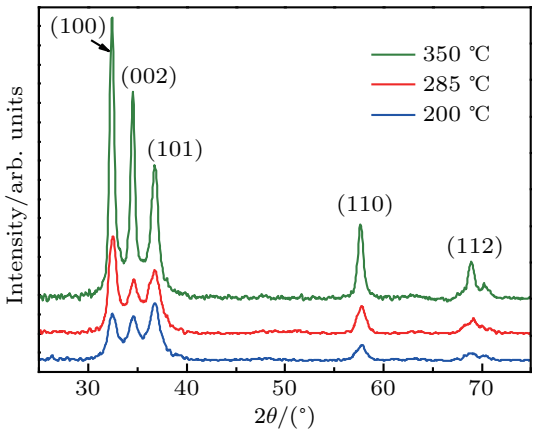


Fig. 2. GIXRD patterns of GaN films grown at 200, 285, and 350 °C.

Based on the optimal deposition conditions, GaN thin films were deposited at various temperatures within the ALD process window. Figure 2 shows the crystalline phases of the GaN films grown at 200, 285, and 350 °C. The Bragg diffraction peaks for these films correspond to (100), (002), (101), (110), and (112) reflection of the hexagonal GaN phase, revealing that the films are polycrystalline with hexagonal structure. It can be seen that the peak intensity increases with elevated growth temperature, indicating an improvement in crystalline quality of GaN due to the increase in mass transport kinetics.[27] In addition, the (100) peak becomes dominant at the deposition temperatures of 285 °C and 350 °C. According to crystallographic symmetry, h-GaN (100) matches better to Si (100) than other reflection planes.

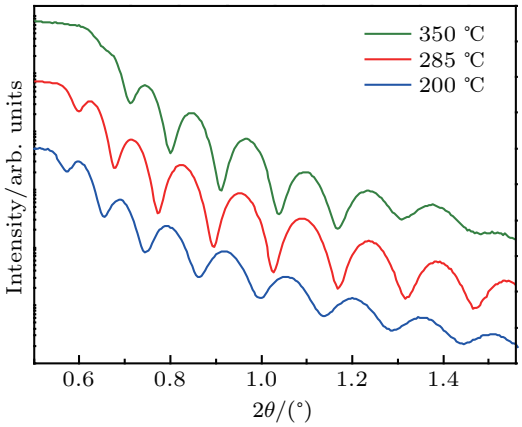


Fig. 3. XRR measurements of GaN films grown at 200, 285, and 350 °C.

It is well known that the interface between epitaxial film

and substrate largely determines the quality of the epitaxial layer. XRR measurements were carried out from the macroscopic area, as shown in Fig. 3. The clearly resolved Kiessig fringes reveal that the interface between GaN film and Si (100) substrate is perfectly smooth. In our previous work, sharp interface between Si (100) substrates and PEALD-grown AlN films has been demonstrated.[26] The obtained sharp interfaces pave a way for post-depositing AlGaN/GaN heterojunctions on Si for GaN-based devices, where the interface between GaN and AlGaN needs to be smooth on an atomic level.

To confirm this feature of sharp interface, TEM was employed to investigate the microstructure of GaN/Si (100) interface. Figure 4(a) shows the cross-sectional HRTEM image of the GaN film deposited at 350 °C. Besides confirming the polycrystalline phase of GaN, the HRTEM image also presents a rather atomically flat interface between the GaN film and Si (100), which verifies the sharp interface revealed by XRR (Fig. 3). From the image, a ∼ 2-nm thick amorphous interfacial layer can be observed at the GaN/Si (100) interface. Figure 4(b) gives a magnified view of the interface area of the same sample. Upon this interlayer, a ∼ 18-nm thick amorphous layer forms followed by polycrystalline GaN. The film thickness is measured as ∼ 54 nm. The selected-area electron diffraction (SAED) pattern of Si (100) is shown in Fig. 4(c).

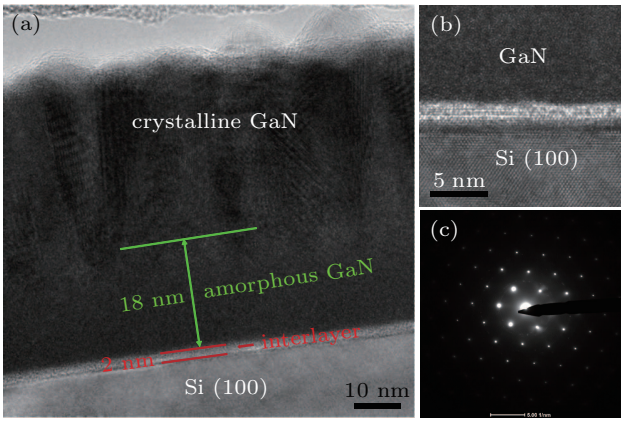


Fig. 4. (a) Cross-sectional HRTEM image of the GaN film grown at 350 °C. (b) HRTEM image of higher magnification of the GaN/Si (100) interface region. (c) SAED pattern of the Si (100) substrate.

To analyze the chemical states of GaN/Si (100) interface, XPS depth profile analysis is provided, as shown in Fig. 5(a). The surface of GaN films was contaminated with oxygen (∼ 25.9%) and carbon (∼ 10.5%), which could arise from atmospheric contamination. The atomic compositions of Ga and N in the bulk film are calculated to be around 32.8% and 58.2%, respectively, which is very similar to the reported values of polycrystalline GaN grown by PEALD.[19] The higher nitrogen content than gallium might result from the plasma-enhanced dissociation of nitrogen during the GaN growth. The XPS survey scan obtained after 1000 s of etch time reveals the elemental composition of the interlayer. The N 1s, Ga 3d, and O 1s XPS spectra are given in Figs. 5(b)–5(c), and 5(d), respectively. Peaks located at 398.9 eV and 397.1 eV, in N 1s spectrum are assigned to N–Ga–O[28] and N–Ga, respectively, and the other two peaks at 395.0 eV and 393.8 eV are determined to be Ga-LMM Auger bonding states.[17,19,29] Peaks at 20.6 eV and 19.9 eV in Ga 3d spectrum (Fig. 5(c)) can be ascribed to the bond of Ga–O,[18] and the Ga–N state is observed at 19.3 eV.[21] Surdu-Bob *et al.* determined that Ga 3d states in Ga_2O_3 have a chemical shift of +0.6 eV on Ga_2O.[30] Therefore, peaks at 530.6 eV and 531.2 eV in O 1s spectra correspond to Ga_2O and Ga_2O_3,[21] respectively. The Si 2p spectra for the etch time of 800 s and 1000 s are shown in Figs. 5(e) and 5(f). It is reasonable to deduce that peaks located at 106.03, 104.75, and 102.83 eV in Fig. 5(f) are the binding energy of Auger-Ga according to the Auger-Ga peaks located at 105.81, 104.26, and 102.45 eV in Fig. 5(e). Peaks located at 98.85 eV and 99.49 eV in Fig. 5(f) are assigned to the binding energy of Si. A feature for Si–O is not present in Si 2p spectra and O–Si bond is not observed in O 1s spectrum, which excludes the native oxides on silicon. These results reveal that the interfacial layer is composed of Ga_xO_y and GaN (or $Ga_xO_yN_z$), which is different from the previously reported SiO_2 interlayer between ALD-deposited GaN and Si substrate.[17] This interlayer with high oxygen impurity concentration worked as a template for further growth. GaN begins as an amorphous film, in which the amount of oxygen decreases with the increasing growth cycles. After ∼ 18-nm thick amorphous GaN has been deposited, crystal nucleation takes place from the amorphous layer. The ratio of oxygen stabilizes to around 6%–8% in the polycrystalline film, which is very close to the reported values of polycrystalline GaN grown by atomic layer deposition.[31] It has been reported that GaN films with large amounts of impurities are amorphous.[18] Therefore, oxygen impurity concentration may have some effect on the crystallization of GaN, and crystal nucleation occurs when the ratio of oxygen drops to ∼ 11% in this case. The high oxygen impurity concentration in interlayer could be a main reason for the formation of amorphous transition layer, whose origin has not been understood. It might from trapped water inside the multilayer coatings on the inner walls of the plasma-enhanced atomic layer deposition vacuum reactor, or it might also from water vapor impurities present in organometallic precursors. More investigations are required to understand the formation of the interfacial amorphous layer and more efforts should be made to prevent the formation of $Ga_xO_yN_z$ interlayer during the GaN film growth.

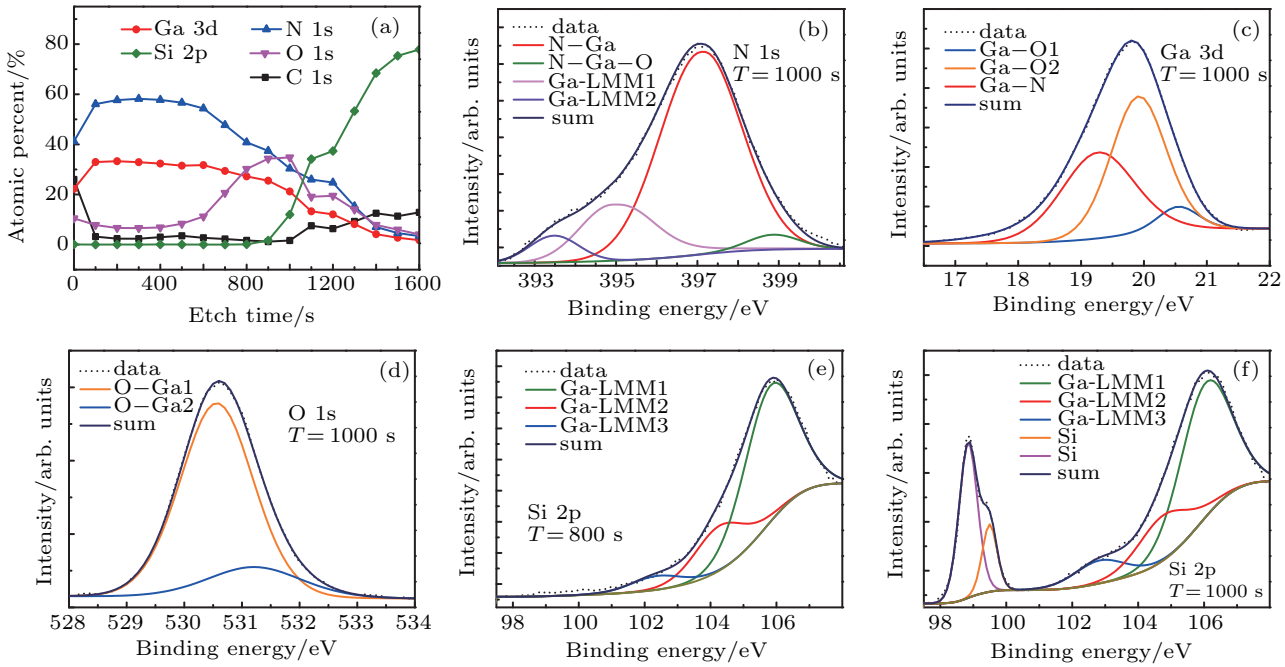


Fig. 5. (a) XPS depth profile of ∼ 54-nm thick GaN layer deposited at 350 °C. High resolution XPS scans of (b) N 1s, (c) Ga 3d, (d) O 1s, and (f) Si 2p for the etch time of 1000 s. (e) High resolution XPS scan of Si 2p in GaN film.

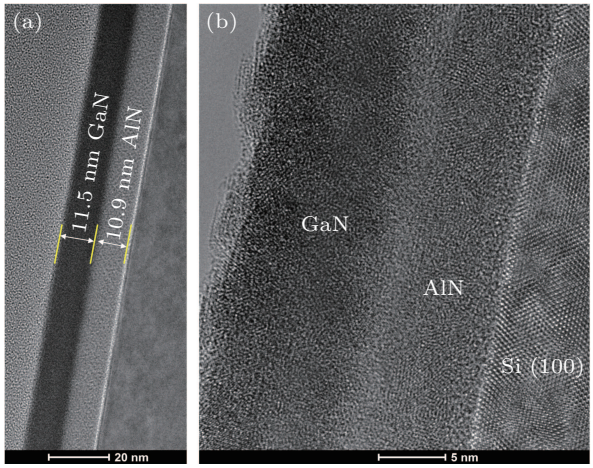


Fig. 6. Cross-sectional TEM images of (a) the 11.5-nm GaN deposited at 350 °C on PEALD-grown AlN/Si (100) and (b) the same sample at higher magnification.

To study the effect of this interlayer on GaN growth, 100-cycle AlN buffer layer was firstly deposited at 275 °C on Si (100) substrate via PEALD and GaN deposition followed. Figure 6(a) shows the cross-sectional TEM images of an 11.5-nm thick GaN grown at 350 °C on a 10.9-nm thick PEALD-grown AlN buffer layer. No interfacial layer is presented at the GaN/AlN interface, and the interfaces at GaN/AlN and AlN/Si (100) are rather flat. Upon this polycrystalline AlN layer, GaN crystallizes after a thin film growth, which can be observed in Fig. 6(b). The polycrystalline phase of this GaN layer is further characterized by GIXRD measurement (Fig. 7), which shows the same diffraction planes of GaN grown directly on Si (100) (Fig. 2). The XPS depth profile (Fig. 8) shows the content of oxygen during the GaN initial growth is ∼ 11%, which is lower than the value of ∼ 34% for GaN grown directly on Si (100) (Fig. 5(a)). These results reveal that the existence of interlayer hinders the crystallization of GaN and give rise to an amorphous transition GaN layer with high oxygen impurity.

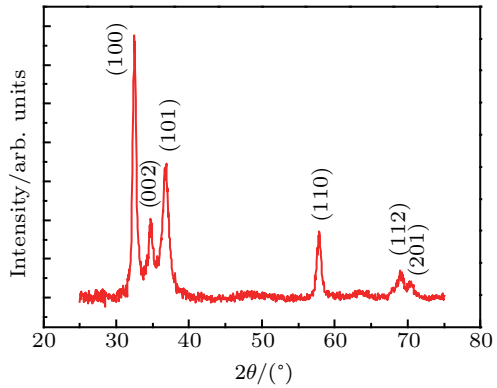


Fig. 7. GIXRD image of the 11.5-nm GaN deposited at 350 °C on PEALD-grown AlN/Si (100).

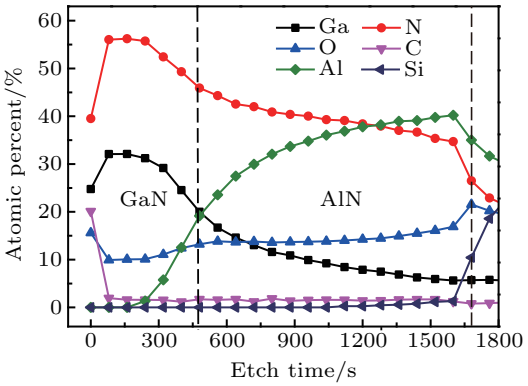


Fig. 8. XPS depth profile of the 11.5-nm GaN deposited at 350 °C on PEALD-grown AlN/Si (100).

After confirming the $Ga_xO_yN_z$ interlayer, XRR experimental data were fitted by using 3-layer model ($GaN/Ga_xO_yN_z/Si$). For GaN grown at 350 °C, the thickness values of GaN film and $Ga_xO_yN_z$ interlayer are estimated to be 52.80 nm and 2.55 nm, respectively, which are in good agreement with the values measured by TEM. The roughness value of interlayer between GaN and $Ga_xO_yN_z$ is found to be 1.31 nm. The density value of 5.36 g/cm^3 extracted from simulations is lower than the recognized value of 6.15 g/cm^3. XRR results also reveal the surface roughness values of GaN grown at 200, 285, and 350 °C are 1.31, 1.64, and 2.3 nm, respectively. To check the surface roughness of the GaN films, AFM was used to analyze the surface morphology of GaN. Figure 9 shows the two-dimensional surface morphologies of the same samples. The root-mean-square (RMS) values of surface roughness measured from 1 μm×1 μm scan area of the samples grown at 200, 285, and 350 °C are 0.90, 0.96, and 1.31 nm, respectively. These values of roughness are reasonably lower than the value estimated by XRR.[17] The increase of surface roughness for GaN grown at higher temperature is due to the effect of the growth temperature in terms of growth speed along different crystallographic directions.[24] These results suggest that the polycrystalline GaN with smooth surface is obtained at different deposition temperatures.

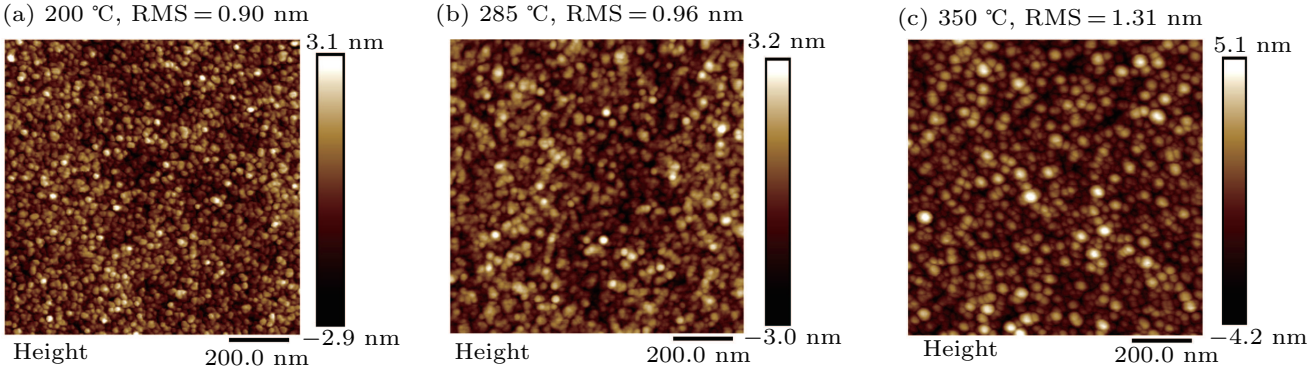


Fig. 9. The 1 μm×1 μm AFM images of GaN films grown at temperatures of (a) 200 °C, (b) 285 °C, and (c) 350 °C.

4. Conclusions

In summary, polycrystalline hexagonal GaN thin films were deposited via PEALD using optimized parameters. Improved crystal quality of hexagonal GaN was obtained at higher temperature due to the increase in mass transport kinetics. GaN films deposited at various temperatures in ALD window present atomically sharp GaN/Si (100) interfaces. However, a ∼2-nm thick amorphous interlayer composed of Ga_xO_y and GaN was formed during the initial growth stage. Then, the formation of an amorphous GaN, in which oxygen impurity concentration decreases from ∼34% to ∼11% with the film growth, and polycrystalline GaN followed. In comparison, GaN deposited on Si (100) by inserting a PEALD-grown AlN buffer layer shows sharp GaN/AlN interface with no interlayer. The oxygen impurity in GaN during the initial growth stage is as low as ∼11%, and GaN crystallizes after a thin film deposition. Hence, it is the $Ga_xO_yN_z$ interlayer that leads to a thick amorphous transition GaN layer with high oxygen impurity concentration and hinders the crystallization of GaN. The obtained sharp GaN/Si (100) interface will be of benefit to the future development of GaN-on-Si technology.

Acknowledgment

The scientific contributions from other people or groups are acknowledged here. Financial supports are given in the footnote on the second page.

References

[1] Walker D, Monroy E, Kung P, Wu J, Hamilton M, Sanchez F J, Diaz J and Razeghi M 1999 *Appl. Phys. Lett.* **74** 762
[2] Mishra U K, Parikh P and Wu Y F 2002 *IEEE Proc.* **90** 1022
[3] Nakamura S, Senoh M and Mukai T 1993 *Jpn. J. Appl. Phys.* **32** L8
[4] Nakamura S, Mukai T and Senoh M 1991 *Jpn. J. Appl. Phys.* **30** L1998
[5] Ikeda N, Niiyama Y, Kambayashi H, Sato Y, Nomura T, Kato S and Yoshida S 2010 *IEEE Proc.* **98** 1151
[6] Nakamura S and Krames M R 2013 *IEEE Proc.* **101** 2211
[7] Hove M V, Boulay S, Bahl S R, Stoffels S, Kang X, Wellekens D, Geens K, Delabie A and Decoutere S 2012 *IEEE Electron Dev. Lett.* **33** 667
[8] Nakamura S, Harada Y and Seno M 1991 *Appl. Phys. Lett.* **58** 2021
[9] Amano H, Sawaki N, Akasaki I and Toyoda Y 1986 *Appl. Phys. Lett.* **48** 353
[10] Lin M E, Sverdlov B, Zhou G L and Morkoç H 1993 *Appl. Phys. Lett.* **62** 3479
[11] Shih H Y, Lin M C, Chen L Y and Chen M J 2015 *Nanotechnology* **26** 014002
[12] Puurunen R L 2005 *J. Appl. Phys.* **97** 121301
[13] Profijt H B, Potts S E, Van d S, M C M and Kessels W M M 2011 *J. Vac. Sci. Technol. A* **29** 050801
[14] Leskelä M and Ritala M 2002 *Thin Solid Films* **409** 138
[15] George S M 2010 *Chem. Rev.* **110** 111
[16] Tekcan B, Biyikli N and Okyay A K 2014 *Opt. Eng.* **53** 107106
[17] Ozgitakgun C, Goldenberg E, Okyay A and Biyikli N 2014 *J. Mater. Chem. C* **2** 2123
[18] Ozgit C, Donmez I, Alevli M and Biyikli N 2012 *J. Vac. Sci. Technol. A* **30** 01A124
[19] Kizir S, Haider A and Biyikli N 2016 *J. Vac. Sci. Technol. A* **34** 041511
[20] Bolat S, Ozgit-Akgun C, Tekcan B and Biyikli N 2014 *Appl. Phys. Lett.* **104** 243505

[21] Alevli M, Haider A, Kizir S, Leghari S A and Biyikli N 2016 *J. Vac. Sci. Technol. A* **34** 01A137
[22] Alevli M, Gungor N, Haider A, Kizir S, Leghari S A and Biyikli N 2016 *J. Vac. Sci. Technol. A* **34** 01A125
[23] Motamedi P and Cadien K 2015 *Rsc Adv.* **5** 57865
[24] Motamedi P, Dalili N and Cadien K C 2015 *J. Mater. Chem. C* **3** 7428
[25] Zhu D, Wallis D and Humphreys C 2013 *Rep. Prog. Phys.* **76** 106501
[26] Liu S, Peng M, Hou C, He Y, Li M and Zheng X 2017 *Nanoscale Res. Lett.* **12** 279
[27] Miikkulainen V, Leskelä M, Ritala M and Puurunen R L 2013 *J. Appl. Phys.* **44** 021301
[28] Eddy C R Jr, Nepal N, Hite J K and Mastro M A 2013 *J. Vac. Sci. Technol. A* **31** 058501
[29] Kushvaha S, Kumar M S, Shukla A, Yadav B, Singh D K, Jewariya M, Ragam S and Maurya K 2015 *Rsc Adv.* **5** 87818
[30] Surdu-Bob C, Saied S and Sullivan J 2001 *Appl. Surf. Sci.* **183** 126
[31] Gungor N and Alevli M 2018 *J. Vac. Sci. Technol. A* **36** 021514